Cleaner Engineering and Technology 26 (2025) 100940

Contents lists available at ScienceDirect

Cleaner Engineering and Technology

journal homepage: www.sciencedirect.com/journal/cleaner-engineering-and-technology

Hydrogen production and import thermal energy recovery and use: a study on water electrolysis waste heat and ammonia cracking cold utilisation

Maxime Philip Kramer [a,*], Klaas-Jan Bosch [b], Kamel Hooman [a]

[a] TU Delft, Process and Energy Department, Delft, 2628CB, the Netherlands
[b] Port of Rotterdam, Rotterdam, 3072AP, the Netherlands

ARTICLE INFO

Keywords:
Ammonia cracking
Water electrolysis
Waste heat recovery
Waste heat use
Cold utilisation

ABSTRACT

The aim of this study is to quantify and utilize waste heat from wind-farm-powered water electrolysers and ammonia cracking. The port of Rotterdam, as a case study, has been analyzed where the transport of 4.6 Mt hydrogen and water electrolysis, powered by wind farms, is planned. A dynamic model was developed to calculate waste heat from an electrolyser powered by fluctuating electricity inputs from offshore wind power. Moreover, thermal analysis of ammonia cracking process streams was conducted. It was observed that integrating water electrolysis waste heat into the ammonia cracking process is not only a promising novel application for the reuse of the electrolysis waste heat, but also it can potentially enhance cracking efficiency by 2 % while creating synergies within the hydrogen industry. Additionally, waste heat can be used for district heating saving more than 70 % of energy and reducing CO_2 by just as much. In parallel, cold utilisation from ammonia cracking was explored for CO_2 and H_2 compression, as well as industrial cold storage to observe that technical implementation is possible.

Nomenclature

Abbreviations	
AD	Adsorption Distillation
CCS	Carbon Capture and Storage
COP	Coefficient of Performance
CS	Cold Side
DN	Diametre Nominal
EU	European Union
HDH	Humidification/DeHumidification
HHV	Higher Heating Value
HS	Hot side
IRENA	International Renewable Energy Agency
LCOH	Levelised Cost of Hydrogen
LHV	Lower Heating Value
LNG	Liquified Natural Gas
LT	Low Temperature
MD	Membrane Distillation
MED	Multi Effect Distillation
MSF	Multi Stage Flash
NO_x	Nitrous Oxides
ORC	Organic Rankine Cycle
RES	Renewable Energy Source
RHS	Right Hand Side
RO	Reverse Osmosis
Constants	
F	Faraday Constant (96 485 C/mol)
R	Gas Constant (8.314 J/K/mol)
Symbols	
α	Charge transfer Coeffient [-]
$\Delta_y T$	Electrolyte stack temperature difference [K]
ϵ	Stack efficiency [-]
η	Efficiency [-]
ρ	Density [kg/m^3]
σ	Electrical conductivity [S/m]
A	Area [m^2]
C_p	Heat capacitance [J/kg/K]
c_p	Heat capacity at constant pressure [J/kg/K]
E	Electric energy [J]
E_a	Activation energy [J]
H	Enthalpy [J]
h	Specific enthalpy [J/kg]
I	Electrical current [A]
i	Current density [A/m^2]
i^0	Exchange current density [A/m^2]
k	conversion coefficient [Bar/mmHg]
m	Molarity [mol/L]

(*continued on next column*)

(*continued*)

(*continued on next page*)

This article is part of a special issue entitled: SDEWES24 published in Cleaner Engineering and Technology.

* Corresponding author.
E-mail address: mmp.kramer@gmail.com (M.P. Kramer).

https://doi.org/10.1016/j.clet.2025.100940
Received 31 January 2025; Received in revised form 17 March 2025; Accepted 20 March 2025
Available online 14 April 2025

(*continued*)

N	Number of cells in stack [-]
n	Amount of substance [mol]
P	Power [W]
p	Pressure [bar]
R	Resistance [Ω]
S	Head loss per pipe length [Pa/m]
T	Temperature [K]
t	Time [s]
U	Potential [V]
U^0	Standard Potential [V]
V_a	Volume [m^3]
$w\%$	Weight percentage [-]
z	Electron transfer number [-]
Subscripts	
a	anodic
bp	bipolar membrane
c	cathodic
cc	current collector
$cell$	cell
e	environment
eff	effective
el	electric
eq	equilibrium
i	–
in	in
$ionic$	ionic
m	membrane
$mesh$	mesh
ohm	ohmic
out	out
$react$	reaction
ref	reference
s	surface
sat	saturation
st	stack
tn	thermoneutral

1. Introduction

According to the International Renewable Energy Agency (IRENA), green hydrogen will play a crucial role in the energy transition (Irena, 2023). The European commission has also recognized this in their hydrogen strategy for a climate neutral Europe (EHB, 2020).

Hydrogen can be produced both at local hydrogen clusters or at large renewable energy source (RES) sites. These RES sites are places where green electricity is relatively cheap (for instance from solar or wind farms), such as the Middle East and countries like Chile, South Africa, Brazil and Namibia (Gasunie, 2024). This cheaply produced hydrogen can then be transported to hydrogen valleys such as Europe, where local production is insufficient and thus imported hydrogen is needed (Port of Rotterdam, 2024). Hydrogen can be transported in its molecular form under high pressure or as a cryogenic liquid. However, research is also being conducted in transporting hydrogen with energy vectors because of the benefits in term of volumetric energy density and less extreme storage conditions (Asif et al., 2023). Ammonia is considered one of the more promising transport molecules for hydrogen (Asif et al., 2023). To recover the hydrogen, ammonia needs to go through a decomposition process.

This study investigates thermal management of the so-called hydrogen valleys, where both local production and import of hydrogen coincide. Inefficiencies in the entire hydrogen value chain (increasing the levelised cost of hydrogen 'LCOH') are still a major hurdle. Recovery and use of thermal waste streams can be used as a way to improve energy efficiency. Modern electrolysers can have a system efficiency of 75.8–77 % and a balance of stack efficiency of 80 % (ISPT et al., 2023), where the unused energy is dissipated as heat. Buttler and Spliethoff, 2018 mentioned utilising waste heat from electrolysers as a way to increase electrolysis system efficiency from 75-80 % to 86–90 %. This electrolysis waste heat utilisation can also decrease CO_2 emissions (van der Roest et al., 2023). Thermal ammonia decomposition (informally known as cracking) does not have a waste heat stream, because all the available heat is used for preheating the ammonia. However, because the ammonia is imported and stored as a cryogenic liquid, utilising the cooling potential as part of the preheating process could be useful. Cold utilisation is a subject of growing interest, especially with the growing use of LNG (He et al., 2019). Cold utilisation improves the exergetic efficiency of the used LNG (He et al., 2019), thus it could have similar potential for the imported ammonia.

Even though in theory water electrolysis is an endothermic process, due to inefficiencies in the system (which cause overpotentials) it still generates significant waste heat. Research on the recovery and use of electrolysis waste heat is limited to pioneering papers with promising prospectives. Reuter and Schmidt, 2022 asses the future waste heat potential of electrolysers and its utilisation in district heating. It shows that use of waste heat from electrolysers could be an important factor in increasing the overall efficiency of these installations and in countries with low heat demand it could completely decarbonize the district heating sector. Buttler and Spliethoff (2018) review the current status of water electrolysis and conclude that further projects are required to investigate the potential for generating synergy effects by integrating waste heat as a by-product. Lastly Böhm et al. (2021) studied sector coupling of electrolysis with district heating. The use of this waste heat for preheating process water, water desalination and district heating networks has been proposed in the literature. Research on the topic of preheating process water has shown that utilising electrolysis waste heat for this scenario only accounts for around 8 % of the heat output (Tiktak, 2019). Water desalination can account for up to 22 % of the total balance of plant costs of electrolysis (Becker et al., 2023), making improvements here valuable. Multiple studies have compared different kinds of water purification techniques in the scope of electrolysis waste heat reuse. Some promising novel, low grade heat, purification techniques (membrane distillation (MD), adsorption distillation (AD) and humidification/dehumidification (HDH)) where highlighted by Elsaid et al. (2020). However, both Tiktak (2019) and González et al. (2017) concluded that reverse osmosis (RO) would still be the preferred option (also compared to the traditional multi stage flash (MSF) and multi effect distillation (MED)). Böhm et al. (2021) analyzed the synergies between water electrolysis and district heating. Both Böhm et al. (2021) and Reuter and Schmidt (2022) concluded that there is large potential to use water electrolysis waste heat for district heating networks in Europe. Accounting for 4 % of the today's EU heating demand by 2030 and 65 % of district heating demand by 2040. Multiple studies have investigated specific cases of combining electrolysers and (LT-) district heating. van der Roest et al. (2023) examines different designs for the utilisation of (waste) heat from a 2.5 MWel polymer electrolyte membrane (PEM) electrolyser. Østergaard and Andersen (2023) study the optimal heat storage in district energy plants with heat pumps and electrolysers. Vidisdottir and Elena, 2022 performed a techno-economic analyses, studying the profitability of green hydrogen production and feasibility of waste heat integration to DHS in the Ísafjörð ur's energy system. Kayali (2023) explores the integration of waste heat from electrolyzers within a Combined Heat and Power plant and district heating network. Pozzetto (2022) provides an analysis of the potential benefits of an electricity - gas - heat integrated energy system, putting extra focus on the waste heat potential from fuel cells and electrolysers. Finally Sommer Hansen and Dokkedal Johnsen (2023) have investigated how power-to-X (in the form of heating systems of Sønderborg). Interestingly, in all of these studies the water electrolysis waste heat only serves as an ancillary heat source. Hermans (2022) did study the feasibility of using a 100 MW wind-powered plant as a main heat source for district heating. From this study it was found that if there is much more heating demand or much less heating demand than the nominal capacity that can be delivered by the electrolysers, heat buffering is not important. However, if heat demand and supply are in the same order of magnitude, heat buffering is crucial.

Cracking of ammonia occurs at elevated temperatures exceeding 500 $^{\circ}C$ (Devkota et al., 2023). Just like water electrolysis, it is an endothermic process, i.e. heat needs to be added to the system. Even though the production and use of ammonia is an established and well developed industry, ammonia cracking for hydrogen production is relatively new. Hence, optimized design and energy management for cracking is called for. Most research on the improvements of ammonia cracking plants have been focused on better catalytic materials, see for instance (Asif et al., 2023), while in parallel, optimizing process streams to preheat incoming gases and maximize efficiency were investigated; as reported in (Devkota et al., 2023).

Because the cracking process occurs at such elevated temperatures, the preheating of feed and fuel streams is very important to improve overall process efficiency. Ammonia is commonly imported as a liquid (Fluor. Port of rotterdam prefeasibility, 2023). This liquid needs to be pressurized and heated from $-33\ ^{\circ}C$ (1 Atm) to the working conditions ($> 500^{o}C$, 30–50 bar).

While the use of waste heat stream has been investigated, difficulties associated with the process were also noted. It is technically impractical to fully recover the waste heat, for instance, due to nitric acid formation in flue gases (ZareNezhad and Aminian, 2011). On the contrary, cold utilisation from the imported ammonia offers significant benefits. Ammonia is already a commonly used refrigerant in energy-intensive industrial cooling processes (compression/absorption refrigeration) (Sanchuli et al., 2024). Moreover, handling ammonia is a routine well established process as it is one of the most produced chemicals on the planet for many decades, thanks to the application of ammonia in the fertilizer industry (Maxwell, 2004). However, no previous studies could be found on cold utilisation of ammonia as hydrogen carrier. Despite that, a study is done regarding ammonia powered ships in need of cooling for cold transport by Zhang et al., 2023. Another study by Lu et al. (2023) considers cold utilisation of an ammonia powered ship to re-liquefy boil-off gas for CO_2 transport. Lastly studies investigating the potential of cold utilisation in LNG evaporation systems are more common, as can be observed in the review of Kanbur et al., 2017.

In view of the above, no prior research has been conducted to investigate ammonia cracking cold utilisation potential. Besides, while ammonia preheating is a very important and energy intensive step in the cracking process, research is focused on reusing internal heat streams. Although this is indeed crucial in maximising efficiency, it could also be beneficial to determine how external waste heat streams could be implemented to contribute in this preheating process. There is more research done on the recovery and use of thermal waste streams of water electrolysis. However, it is often the same few applications that are researched in different contexts. Considering hydrogen valleys where import and production of hydrogen will work in tandem, it could not only be valuable to utilize all available thermal energy, but especially if reused within the different parts of the hydrogen value chain.

Hence, the aim of this study is to fill these gaps in the literature and unleash the potential of hot and cold streams in hydrogen valleys where green hydrogen is produced and imported using ammonia as the career for hydrogen. This will be done by using the port of Rotterdam in the Netherlands as a case study for a hydrogen valley. The Port of Rotterdam Authority is targeting to become the 'Hydrogen Hub' for Northwestern-Europe where, through a combination of production and import, transport of 4.6 Mt H_2 in 2030 (Port of Rotterdam, 2025) and 20 Mt H_2 in 2050 (Port of Rotterdam, 2025), through the port, is materialized. The initial step is to install offshore wind-powered electrolysers with a capacity of 2–2.5 GW in 2030 (to be expanded to 20 GW by 2050). On top of this generation capacity, excess hydrogen is to be imported as ammonia. Thanks to this concurrent transport and generation of hydrogen, the port of Rotterdam offers an interesting case study.

To achieve this goal, first numerical models are used to determine how much electrolysis waste heat and ammonia cooling potential are available. Those results are then used to compare different applications for those thermal waste streams. For the electrolysis waste heat, the novel application of integration in the ammonia cracking process will be compared to integration in a district heating network. Integration in ammonia cracking is interesting as it is not only a novel application, but also one that potentially combines hydrogen import and production. District heating is a socially relevant application that has shown potential in among others the studies mentioned in previous paragraphs. The ammonia cracking cooling potential will be studied for intercooling of (H_2 and CO_2) gas compression and industrial cold storage applications. H_2 and CO_2 gas compression are relevant because of the expected electrolysis (Port of Rotterdam, 2025) and CCS (Porthos project (Porthos. Porthos info, 2024)) projects in the port area. As a lot of cooled goods are transported through the port, there are multiple cold storage warehouses. This could also be a trivial, but useful application.

2. Modelling

Matlab Simulink was used for modelling and the equations used for this purpose are as per the following sections.

2.1. Electrolysis waste heat

The electrolysers in the port of Rotterdam will be powered with offshore wind power. In order to determine the available wind energy, a simple wind to power conversion model has been made. Wind data was gathered from a publicly available measurement campaign from TNO (from K13A-site, 2022) (TNO. Offshore wind data, 2024). The wind-power curve of the Vestas V164-8 MW was used for the conversion of this wind data into power (Desmond et al.). The generated wind power is then used as input for the considered alkaline electrolyser (currently being implemented in the first large scale electrolysis plant in port of Rotterdam) where the water to hydrogen conversion, generates waste heat.

In this first plant, the Thyssenkrupp Nucera Scalum (Thyssenkrupp nucera, 2023) electrolyser will be used. However, not enough data is (publicly) available, thus the modelled electrolyser will also use information from the one GigaWatt electrolyser project (ISPT et al., 2023). This results in the electrolyser design shown in Fig. 1 wherein the stack geometry and cell design are schematically depicted.

2.1.1. Electrochemical modelling

The model consists of two parts, the electrochemical and the thermal part. The goal of the electrochemical part of the model, is to determine the polarisation curve, the thermoneutral potential and the amount of gases produced. The electrochemical part is modelled as a static model. This is done because the timescale in which transient effects occur is so small that electrochemical equilibrium is achieved in the order of milliseconds (Olivier et al., 2017). Compared to the timescales used in each step in the simulation (based on the wind data), it is a safe assumption to model the electrochemical model as static.

Equation (1) is used to calculate the total cell potential. This results in the eventual polarisation curve. A combination of analytical and empirical equations is used to construct a basic polarisation curve. At the end, parameters of this model are adjusted to resemble a known polarisation curve in order to closely represent the reference electrolysers.

$$U_{cell} = U_{eq} + U_{act} + U_{Ohm} \tag{1}$$

To determine the equilibrium potential, the first term in the right-hand-side (RHS) of Equation (1), the Nernst equation, Equation (2), is used:

$$U_{eq} = U^{0} + \frac{RT}{nF} ln\left(\frac{\alpha_{H_2}\alpha_{O_2}^{0.5}}{\alpha_{H_2O}}\right) \tag{2}$$

Wherein U0 is the formal potential and is the minimum amount of energy required for the electrolysis reaction to occur. The formal potential is proportional to the Gibbs free energy (see Equation (3)). For

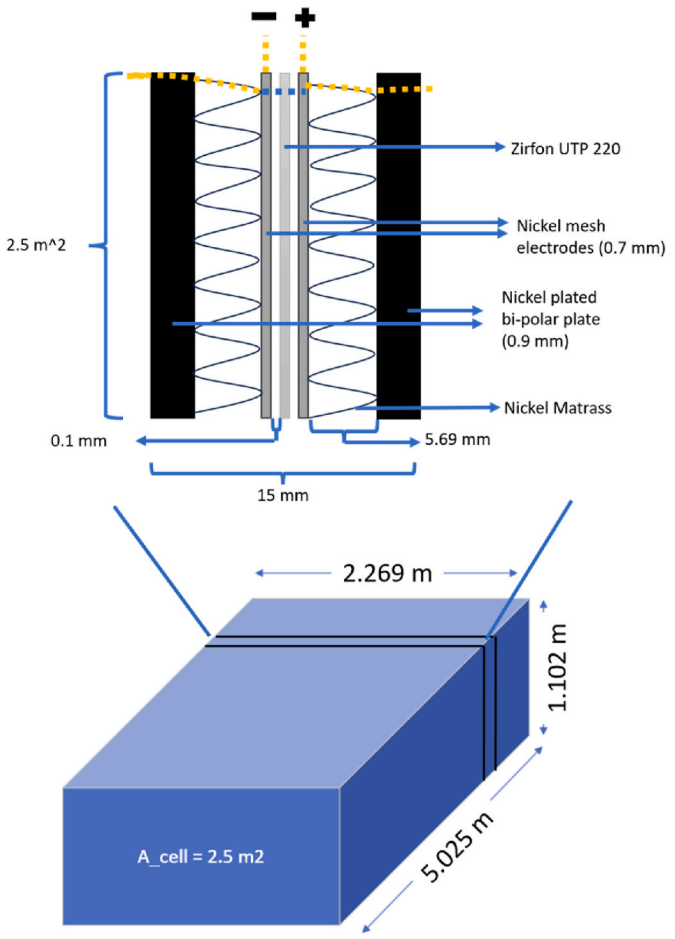

Fig. 1. Schematic representation of modelled electrolyser showcasing the stack geometry and cell design. The yellow dotted line represents electron flow through the cell and blue dotted line represents OH^-.

the model, a commonly used empirical relation has been implemented (Equation (3)). The terms α^H, $\alpha^{0.5}$ and α_0^H are the activities of the different species in the reaction. For the product gasses, the activities are equal to their partial pressures. Pure liquid water has an activity of 1, however, because the water is not pure (but mixed with KOH) the activity changes. This change in activity as a function of molar electrolyte concentration m (mol/L) and temperature T (Kelvin) is given by the empirical formula Equation (4) (Hu et al., 2022).

$$U^0 = -\frac{\Delta G}{zF} = 1.5184 - 1.54211e-3\ T + 9.523e-5\ T\ ln(T) + 9.84e-8\ T^2 \quad (3)$$

$$log(\alpha_{H_2O}) = -0.02255\ m + 0.001434\ m^2 + \frac{1.38\ m - 0.9254\ m^2}{T} \quad (4)$$

The second term in RHS of Equation (1) is the activation overpotential. The activation overpotential arises from the kinetics of the electronic charge transfer reactions and is defined as the difference between the electrode and electrolyte potential. This overpotential can be represented for the anode and cathode as Equation (5) and Equation (6), respectively.

$$U_{act,a} = \frac{RT}{\alpha_a F} ln\left(\frac{i}{i_a^0}\right) \quad (5)$$

$$U_{act,c} = \frac{RT}{\alpha_c F} ln\left(\frac{i}{i_c^0}\right) \quad (6)$$

In the above equations (Equation (5) and Equation (6)), the α and i^0 terms still need to be determined. The former represents the charge transfer coefficient and for single electron transfer reactions it follows Equation (7). These often tend towards symmetry when the rate-determiningstep is the first single-electron transfer step and is therefore generally assumed to be 0.5 (Haverkort, 2024). However, water splitting is a multi electron transfer process. Depending on the rate determining step (which among others is dependent on electrode conditions) the charge transfer coefficients have different values. This is often denoted as the effective charge transfer coefficient α_{eff}. The value of α_{eff} is important for the value of the tafel slope. The i^0 term is the exchange current density and strongly influences the value of the activation overpotential. The exchange current density is dependent on many factors such as electrode material, temperature and type of electrolyte. If a reference exchange current density is known, this reference value can then be used in Equation (8) to determine the right exchange current density for the operating conditions. The final values for α_{eff}, i_c^0 and i_a^0 are 0.45, 1000 A/m2 and 100 A/m^2 respectively. These values have been chose so that the polarisation curve in Fig. 2 matches the reference curve as closely as possible.

$$\alpha_a + \alpha_c = 1 \quad (7)$$

$$i^0 = i_{ref}^0\ exp\left[\frac{E_a}{R}\left(\frac{1}{T_{ref}} - \frac{1}{T}\right)\right] \quad (8)$$

The last term in Equation (1) is the ohmic overpotential caused by the electronic and ionic resistance of the system. The total resistance can be modelled as the sum of the individual layer resistances. The flow of electron and ionic charge is represented with the dotted lines in Fig. 1. The resistance of each separate component is not only dependent on the conductivity, but also on geometric parameters as the layer thickness t and cell area A_{cell}.

$$R_{bp} = \frac{t_{bp}}{A_{cell}\ \sigma_{bp}} \quad (9)$$

The electrical resistance of the bipolar plate (R_{bp}) is determined using Equation (9). The steel bipolar plate is nickel plated and the conductivity of the steel bipolar plate can be modelled as σ_{bp} is 1.45e + 6 [S/m] (Thoughtco. steel conductivity, 2024).

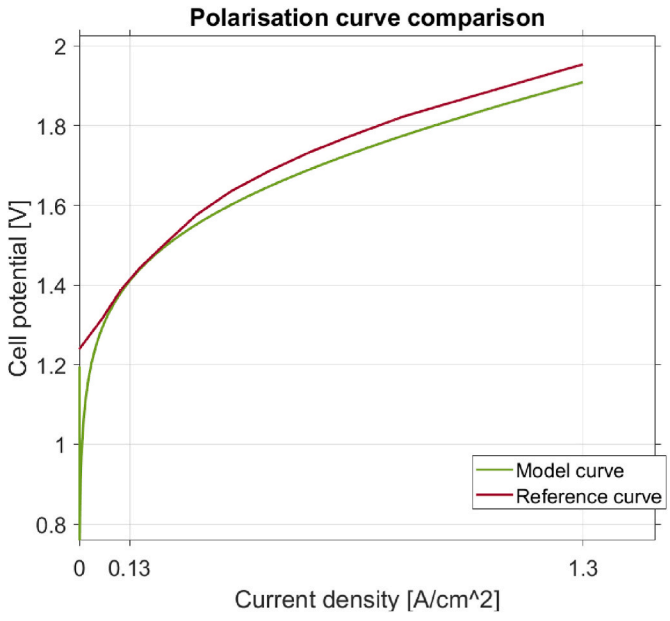

Fig. 2. Polarisation curve.

$$R_{mesh} = \frac{t_{mesh}}{A_{mesh}\ \sigma_{mesh}} \tag{10}$$

The mesh resistance, see Fig. 1, is given by Equation (10) where t_{mesh} is 5.69 mm and σ_{mesh} is the same as that for the current collector (same material). The exact geometry of the mesh is not known, therefore A_{mesh} is adjusted to match the polarisation curve from De Nora (De Nora, 2024) in Fig. 2. The final value of A_{mesh} is 0.208 cm^2.

$$R_{cc} = \frac{t_{cc}}{A_{cell}\ \sigma_{cc}} \tag{11}$$

The resistance of the current collectors (R_{cc}), which in this case are the nickel meshes, is given by Equation (11). The conductivity σ_{cc} of the nickel meshes is given by (24):

$$\sigma_{cc} = 60000000 - 279650\ T + 532\ T^2 - 0.38057\ T^{-3} \tag{12}$$

$$R_{el} = \frac{t_{el}}{A_{cell}\ \sigma_{el}} \tag{13}$$

$$\sigma_{el} = -2.04\ m - 0.0028\ m^2 + 0.005332\ m\ T + 207.2\ (m/T) + 0.001043\ m^3 - 0.0000003\ m^2\ T^2 \tag{14}$$

Lastly the resistance of a 0.22 mm thick Zirfon membrane (R_m) can be determined using Equation (15). The ionic resistance term R_{ionic} can be determined as a function of the temperature (AGFA).

$$R_m = \frac{R_{ionic}}{A_{cell}} \tag{15}$$

After the Zirfon membrane, all previous steps are repeated for the second half of the cell. The total ohmic overpotential can then be determined using the following equation:

$$U_{ohm} = (2R_{bp} + 2R_{cc} + 2R_{el} + R_m)\ I \tag{16}$$

As mentioned at the beginning, the goal of modelling the cell potential is to able to construct the polarisation curve, which is the temperature and pressure dependent relation between the applied current density and cell potential. The Scalum electrolyser uses electrolysis cells made by De Nora (De Nora, 2024). These are advanced alkaline electrolysis cells. In order for the modelled cell potential to match the De Nora cell polarisation curve; α_{eff}, i_{ref} and nickel mattress area have been adjusted to match the advanced polarisation curve, resulting in the polarisation curve shown in Fig. 2.

In order to determine how much H_2 is being produced, Faraday's law for electrolysis can be used, see Equation (17). In this equation, η_F is the faradaic efficiency, which represents losses due to parasitic currents and unwanted side reactions. N is the number of cells in the stack (335 in series). For the H_2 production the electron transfer number z = 2, for the oxygen production z = 4. F is the Faraday constant. A faradaic efficiency of 98 % is assumed. Only at very low current densities (order of magnitude 10 mA/cm^2), the faradaic efficiency starts to significantly drop (Yodwong et al., 2020). At nominal current densities of modern alkaline electrolysers, faradaic efficiency is reported to be in the range of 98 %–99.9 % (Buttler and Spliethoff, 2018). However, because the exact data for the modelled electrolyser is not available and intermittent/partial load operation (which increases shunt current and in term decrease Faraday efficiency (Sakas et al., 2024)) are an important part of this study, a more conservative approach of 98 % is used.

$$\dot{n} = \eta_F \frac{IN}{zF} \tag{17}$$

The produced gases do not only contain H_2 and O_2, but also some water vapor. The mass of evaporated water can be determined using Equation (18). This equation originates from Dalton's law of partial pressures to determine gas mixture compositions. In this equation $\dot{n}$ other are either the H_2 or O_2 production (depending on electrode). P_{sat} is the water saturation pressure given by the Antoine equation (Equation (19)) and $P_{electrode}$ is the electrode pressure (1.3 Bar). In this model no gas crossover is assumed.

$$\dot{n}_{H_2O} = \dot{n}_{other}\ \frac{p_{sat}}{p_{electrode} - p_{sat}} \tag{18}$$

$$p_{sat} = k\ 10^{A - \frac{B}{C+T}} \tag{19}$$

For water between 273 K and 373 K, the coefficients A,B and C are respectively 8.07131, 1730.63 and 233.426. The numerical value of coefficient k for unit conversion from mmHg to Bar is (k = 0.001333).

In order to determine how much heat is actually produced during the electrolysis process, the thermoneutral potential is crucial. The amount of waste heat is directly proportional to U_{cell}-U_{tn}. The thermoneutral potential is proportional to the enthalpy change ΔH, as

$$U_{tn} = -\frac{\Delta H}{zF} \tag{20}$$

The value of ΔH^0 is −283 kJ/mol at standard conditions (1 atm, 298 K), resulting in U_{tn} = 1.48V. However, the pressure and temperature conditions in the electrolyser are different and dynamic. U_{tn} is determined by calculating the enthalpy change of in- and out-going streams in relation to the standard conditions for which the reaction enthalpy ΔH^0 is known (see Equation (21)). Also, the enthalpy change due to evaporating water is taken into account. All the enthalpy values in the electrolyser model have been calculated using the NIST REFPROP software (Lemmon et al., 2018).

$$\Delta H_{react} = \Delta H^0_{react} + \Delta H_{in} - \Delta H_{out} \tag{21}$$

2.1.2. Thermal modelling

The electrochemical part of the model has been described, which determines the cell potential and thermoneutral potential. The difference between the two is the produced waste heat (see Equation (24)), which can now be coupled to the dynamic thermal part of the model. The thermal behavior of the stack can be modelled as a lumped thermal capacity model. It is assumed that temperature changes are uniform throughout the stack. This is generally assumed for electrolyser with thin cell layers where the electrolyte flows through the entire stack (Olivier et al., 2017). The thermal balance of the stack is given by Equation (22).

$$C_{p,st}\frac{dT}{dt} = Q_{produced} - Q_{loss} \tag{22}$$

The stack thermal capacitance $C_{p,st}$ is important for the thermal behaviour as it dictates how much energy is needed to heat up by a certain temperature. According to measurements from Diéguez et al. (2008), the stack and gas-liquid separator are the most crucial in dictating the temperature fluctuations. Taking these into account to calculate the thermal capacitance using Equation (23), gives a value of 62089 kJ/K. This is in agreement with a calculation of a similarly sized electrolyser in (Sakas et al., 2022).

$$C_{p,st} = \sum c_{p,i}\ V_i\ \rho_i \tag{23}$$

The produced heat is calculated with Equation (24). N is the amount of cells in the stack and I the total current. $Q_{evaporation}$ is the amount of produced heat that is absorbed by the process water that evaporates during the electrolysis process.

$$Q_{produced} = (U_{cell} - U_{tn})\ N\ I - Q_{evaporation} \tag{24}$$

Losses to the environment are dominated by convective and radiation heat transfer (Diéguez et al., 2008). To minimize these heat losses, a layer of insulation is assumed. The insulation is also beneficial for the start up and cool down characteristics of the system (faster heating time and slower cooling time). These losses are represented in Equation (25). A_s is the total exterior surface area of the stack and h_{total} is the total surface-air heat transfer coefficient. The numerical value for this heat transfer coefficient for an alkaline electrolyser has been experimentally

determined to be 4.3 W/m^2/K (Diéguez et al., 2008). T_s is the stack temperature and T_e is that of the constant ambient air (which is assumed to be 283 K in this paper).

$$Q_{loss} = h_{total}\, A_s\, (T_s - T_e) \tag{25}$$

Cooling of the stack happens by an excess amount of electrolyte flow through the cell (this control process is not modelled). For every time step, if the temperature is at operating temperature (353 K), the amount of waste heat produced is given by Equation (26). Q_{vapor} is the regained heat energy from the gases and water vapor. Which are assumed to be cooled back down to 323 K using the closed circulating cooling loop (Fig. 3). If the stack temperature is below the operating temperature of 353 K, no waste heat is recovered. Q incoming process water.

$$Q_{waste-heat} = Q_{produced} + Q_{vapor} - Q_{loss} - Q_{preheat} \tag{26}$$

It is important to know at what temperature the waste heat can be collected. To do that Equation (27) is used wherein T_o is the output temperature. Here the value $\Delta_y T$ is the temperature difference between stack and electrolyte. The variable T is the stack temperature. For this research the $\Delta_y T$ value will be kept at a constant 3 K (Tiktak, 2019).

$$T_o = T - \Delta_y T \tag{27}$$

The distribution of waste heat from the electrolyser to a consumer is expected to be indirect and through multiple steps. First the electrolyte needs to go through a heat exchanger to the closed circulating cooling loop that cools the electrolyte. Then through another heat exchanger to deliver the heat to the distribution pipes. Then it travels through the distribution pipe. Lastly is passes through another heat exchanger from the distribution pipe to the distribution network of the heat consumer. This process is illustrated in Fig. 3. There are multiple heat exchangers in the transport network. For this application specifically, a counter flow plate heat exchanger, with temperature drop of 3 K, is selected (Le Coultre, 2022). A temperature loss of 1 K has been assumed for the hot side of the transport pipe, based on pipeline manufacturer estimates (Isoplus design manual). This temperature loss corresponds to a DN1000 pipeline of 30 km. This length has been chosen because the transport pipelines used for district heating will have a smaller range.

2.1.3. Electrolyser plant

The model that has been described until this point, has been based on a 20 MW setup. The total expected nominal capacity at the port of Rotterdam is 2 GW. The first electrolyser plant that is being built will have a nominal capacity of 200 MW, thus it is assumed that the total 2 GW consists of 10 × 200 MW plants. A 200 MW plant will be made up of 10 parallel modular 20 MW electrolysers each of which modelled here.

2.2. Ammonia cracking cold utilisation

In order to determine the cooling potential of ammonia, it is important to know the quality of the thermal stream and the corresponding amount of energy per unit mass of ammonia. The operating conditions have an effect on the state of ammonia entering the plant.

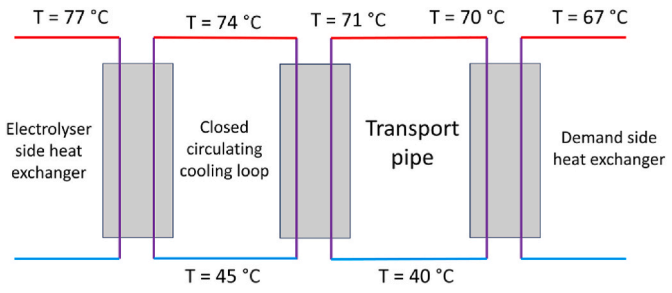

Fig. 3. Schematic depicture of distribution electrolysis waste heat.

This plays a role in the heating profile of the ammonia, which influences what type of heat source can be used to heat up ammonia (i.e. the cold utilisation). This section explains how the quality and quantity of the thermal streams for ammonia are calculated and used to generate heat profiles.

In order to determine the quantity of (heat) energy that can be absorbed by the ammonia stream, the enthalpy difference between the before- and after-heating state needs to be determined. This is dependent on both temperature and pressure. The CoolProp (Bell et al., 2014) library in python is used to make these calculations.

After the quantity of energy is determined, its influence on the thermal stream temperature (while heating) can be determined. Fig. 4 shows a p-h plot of ammonia. For utilising the cooling potential of ammonia, preferably the evaporation enthalpy is used to absorb the heat, this large energy absorption over a small temperature difference results in compact sizing of heat exchangers needed for the heat transfer. The end usage of ammonia, in this case ammonia cracking, should also be taken into consideration. Ammonia cracking commonly occurs at elevated pressures of 30–50 bar (Fluor. Port of rotterdam prefeasibility, 2023). From this perspective, as illustrated in Fig. 4, the liquid stored ammonia is pumped to a higher pressure. As seen, the green path (pumping + heating) needs much less energy to elevate the pressure than the orange path (heating + compression). Moreover, for pumping no intercooling is required (as opposed to compression). In the pumping scenario, the amount of heat that can be absorbed by the ammonia is nearly identical at both 30 and 50 bar (up until the 2-phase region). When used directly, the high pressure ammonia should still be able to cool substances down close to its evaporation point of -33^oC. Although much bigger heat exchangers are needed compared to evaporative cooling.

By determining the different process streams, a simplified model of the ammonia cracking process is created to construct a composite curve, which can then be used to determine how much heating (at specified temperatures) can be integrated. First the different process input streams are determined (CS 1 + 2). This has been done by using data from an internal pre-feasibility study (Fluor. Port of rotterdam prefeasibility, 2023). A summary of the different process streams is shown in Table 1 The first cold stream is the input ammonia, which enters the system at $-33\ ^\circ C$, 30 bar (after pumping) and is heated to the process temperature of $600\ ^\circ C$. The composition of the first hot stream, which is the cracked gas, has been determined by using ASPEN plus V12 (Aspen

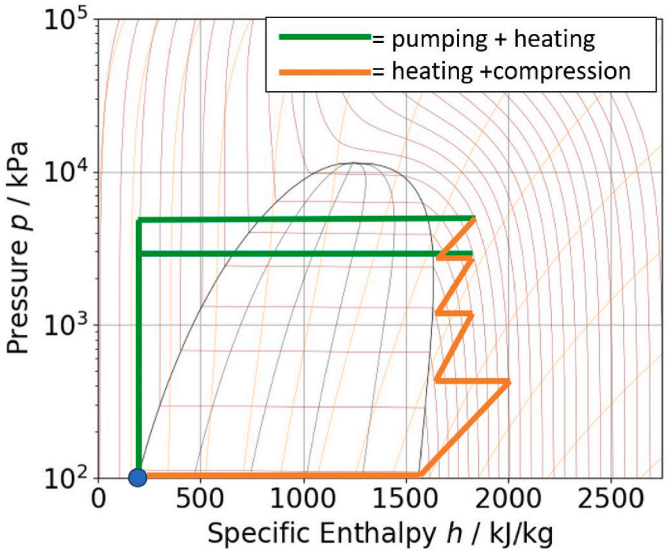

Fig. 4. Different paths of ammonia compression and heating. Blue dot indicates storage conditions. Green path is first pumping and then heating. Orange path is first evaporation and then compression.

Table 1
Table with process stream values of ammonia cracking process. These values correspond to a cracking plant that uses 20.6 kt of ammonia per day, producing 2.92 kt of H_2 per day, thus assuming a system efficiency of 90.3 %. CS = Cold stream, HS = Hot stream.

Process streams	What?	Composition [w %]	Temperature range [^oC]	$\dot{m}$ [kg/s]
CS 1	NH3	100 % NH3	−33 to 600	238
CS 2		H2: 2.4	20 to 800	304
	fuel gasses	N2: 73.0		
		NH3: 2.2		
		O2: 22.4		
HS 1	Cracked gasses	NH3: 2.84	600 to 30	238
		N2: 72.92		
		H2: 17.25		
HS 2	Flue gas	N2: 74.8	800 to 80	304
		H2O: 25.2		

Technology Inc, 2024) (see Fig. 5). A simple Gibbs reactor has been used to determine the composition and heat of reaction at the specified conditions (3111.4 kJ/kg NH_3). This information can then also be used to construct the second cold stream (the fuel for the furnace). The fuel consists of recycled ammonia and H_2 from the cracking process and is mixed with air. The air is modelled as a mixture of only oxygen and nitrogen (and quantities match stoichiometric conditions for complete combustion). All of the ammonia is recycled and for the remaining fuel demand, recycled H_2 for the combustion process is varied to accommodate the total heat demand (reaction energy requirement of cracking process + hot utility requirement). Again ASPEN is used to model the furnace output heat at given conditions (1 bar, 800 ^oC flue gas, Fig. 5). The second hot stream is the flue gas. This gas is cooled down only to 80 ^oC (lower temperature is not advised as nitric acid dew point is 54 ^oC (ZareNezhad and Aminian, 2011)). When the flue gas is cooled lower than this temperature, water condenses in the flue gas and reacts with the NOx emissions in the flue gas to form nitric acid. If nitric acid is formed it can badly corrode the plant equipment, thus this should be avoided. The Coolprop library (Bell et al., 2014) is then used to determine the heat supply/demand of the different process streams in order to construct the T-Q diagrams of the process (Fig. 6). This is used both to calculate how much cooling can be delivered for cold utilisation purposes and also for electrolysis waste heat purposes. The distribution of cold utilisation will be discussed in the next section, as it is very case dependent.

3. Case descriptions

3.1. District heating

A previous feasibility study by Port of Rotterdam Authority (Royal haskoning, 2022), indicated that waste heat could be supplied to district

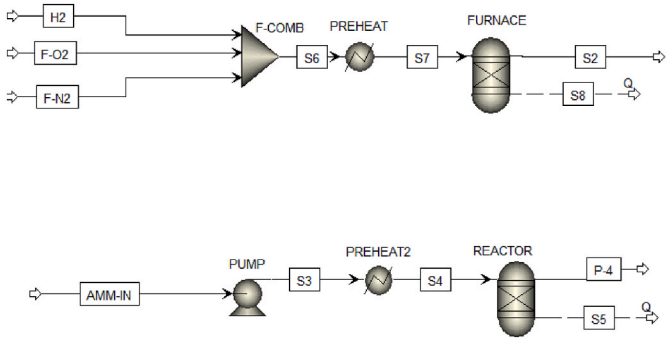

Fig. 5. Aspen schematic setup. The above process models the furnace. The below process models the reactor.

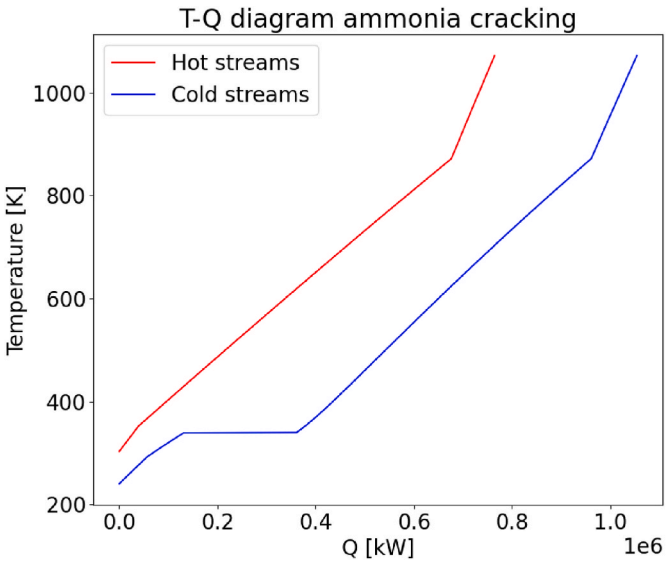

Fig. 6. Composite curve of modelled ammonia cracking process.

heating networks either connected to urban areas, or to greenhouse industry (see Fig. 7). There is a lot of intermittent behavior both at the demand and supply side of the heating network. Hence, the infrastructure (transport pipes, buffer storage and flexible heating as schematically depicted by Fig. 8), plays a crucial role.

With district heating for urban areas, the municipalities Voorne-Putten, Brielle, Rockanje and Hellevoetsluis are used for the heating demand, based on previous feasibility studies by Port of Rotterdam Authority. In order to determine this demand, a tool developed by TNO is used (TNO. Warmteprofielengenerator, 2022), which calculates the hourly heating demand (Fig. 9). For the urban areas, a transportation pipe of size DN450 is selected. The storages are daily storages with capacities matching 12 h average demand (0.57 and 1.56 GWh respectively for storage 1 and 2).

Alternatively, the greenhouse industry in the Westland and Oostvoorne areas have been indicated as another potential waste heat consumer in the previous feasibility study by Port of Rotterdam Authority. These areas cover a total of 25e+6 m^2 (CBS. oppervlakte westland, 2024). The heating demand from these areas is shown in Fig. 10 and the profile is constructed by displacing a seasonal heating profile (Royal haskoning, 2022) with a normalized heating degree day profile. For the

Fig. 7. Schematic of possible district heating near the port of Rotterdam. Fruit icons indicates the greenhouse areas and house icons indicate house areas. The red lines indicate the tracés for transport lines.

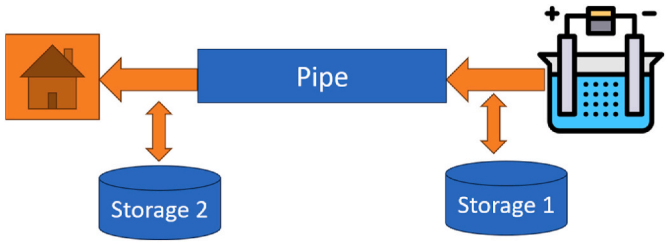

Fig. 8. Schematic of electrolysis waste heat transport for district heating.

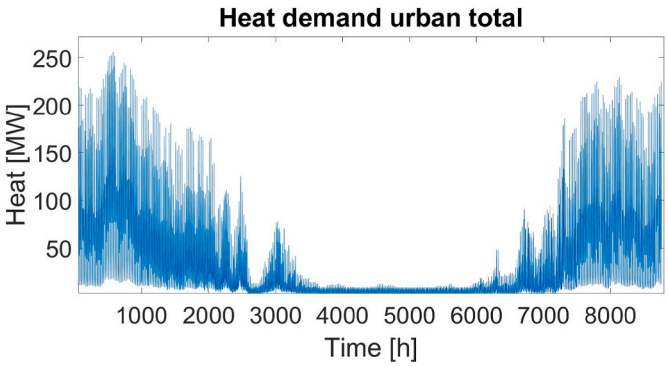

Fig. 9. Total heating demand urban areas.

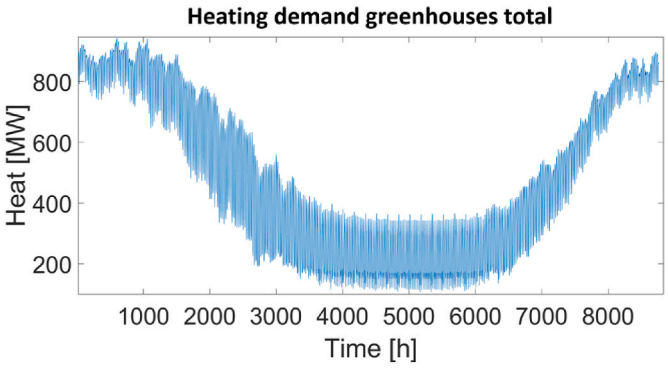

Fig. 10. Total heating demand greenhouses.

distribution of waste heat to greenhouses, a distribution pipeline sized DN800 is selected. The storages are daily with capacities matching 12 h average demand (2.6 and 9.6 GWh respectively for storage 1 and 2).

The tapwater needs to be heated to at least 60 $°C$ (van der Roest et al., 2023). Assuming a bit of heat loss in the distribution network and a heat exchanger between the network and individual systems of each delivery system, it will be assumed no further heat upgrading (heat pump) will be needed (based on the previously determined temperature losses). Greenhouses also fall within the right range with demand temperatures falling between 60 and 70 ^oC (Royal haskoning, 2022).

3.2. Cracking heat integration

The waste heat can alternatively be integrated into the ammonia cracking plant. The heat supply assessment follows the same modelling steps as those for the district heating. Besides, the heat distribution will be in the same temperature range (40–70^oC). Nonetheless, one key difference is that the infrastructure will not pose a significant burden mainly because different industries will likely be placed (physically) close to each other.

3.3. Gas compression intercooling

There are two relevant gas compression applications in the port of Rotterdam; CO_2 compression and H_2 compression. The use of thermal streams in these two processes will be investigated here.

3.3.1. CO_2 compression

Porthos is a large CCS project under construction in the port of Rotterdam. The goal of project is to capture CO_2 from different industries in the port and store it in an underground storage. The aim is to store around 2.5 Mt of CO_2 per year over a period of 15 years. The gas will be compressed to 130 bar before storage (Porthos. Porthos info, 2024).

The conventional method for compressing CO_2 is compression with refrigeration for sub-cooling and pumping. However, novel methods exist that aim to reuse thermal streams to optimise the compression. Mostly ORC's and absorption refrigeration are used for this. A study done by Jackson and Brodal (2018) showed that, if optimized, the total specific power consumption between the different techniques is negligible. There is an exception: when a cold source is available, then conventional compression would be the preferred method (which is the case here).

The Porthos compressor station admits the incoming gas at 35 bar and compresses it to 130 bar with an isentropic efficiency of 0.85. The pressure ratios follow the design of Jackson and Brodal (2018), resulting in three stages. The last stage is at 10 bar above its critical pressure (=83.9 bar). A p-h graph representation of both processes is shown in Fig. 11.

From the compression process presented for CO_2 compression (Fig. 11), the temperature ranges between 283 and 337 K. In order to deliver the cooling potential from the ammonia cracking plant to the gas compression intercoolers, water will be used as a medium to carry this energy. The reason for this is that the different facilities are likely not close to each other and transporting pressurized, low temperature, toxic ammonia is not preferred. Energetic values for compression and cooling are shown in Table 2.

3.3.2. H_2 compression

The hydrogen that will be produced by both the electrolysis and ammonia cracking will have to be compressed to 50 bar for transport (Hynetwork, 2024). Because the ammonia cracking process already occurs at high pressures, the formed ammonia does not need a lot of compression. Hydrogen produced during electrolysis is formed at lower pressures and needs compression. There are different methods of compressing hydrogen, which can be divided in both mechanical and non-mechanical compression (Sdanghi et al., 2019). Mechanical

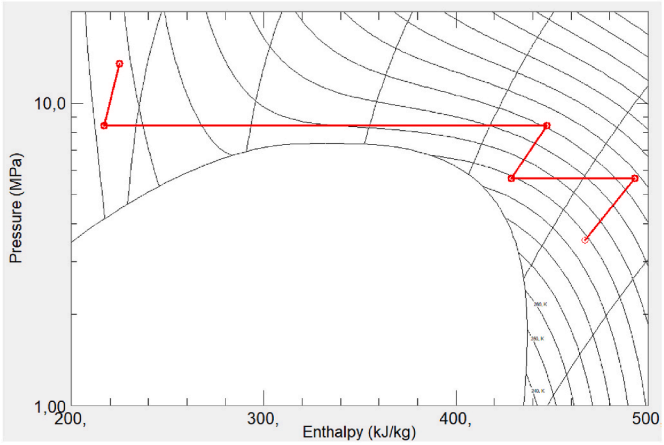

Fig. 11. CO_2 compression and pumping process of 35–130 bar. The plot was made with NIST REFPROP (Lemmon et al., 2018).

Table 2
Energetic values for compression and cooling of CO_2. Specific energy has been determined with Fig. 11, and CO_2 massflow of 79.27 kg/s is used (Porthos. Porthos info, 2024). For the power calculation of the cooling energy, a COP of 3.78 is used (Jackson and Brodal, 2018). The mean power and yearly usage are the electrical energy input.

	Δh CO_2	Mean power	Yearly usage
Compression	49.19 kJ/kg	3.90 MW	3.42e+4 MWh
Cooling	291.41 kJ/kg	6.11 MW	5.33e+4 MWh

compression methods (for H_2 mainly reciprocal compressors) are generally considered (Witkowski et al., 2017).

The engineering design for the hydrogen compression will be based on Witkowski et al., 2017, in which a comprehensive analysis of hydrogen compression was done for pipeline transport. A compression ratio of 1.71 and isentropic efficiency of 0.85 are used to construct the compression shown in Fig. 12.

From the compression process presented for H_2 compression, the temperature ranges between 303 and 362 K. In order to deliver the cooling potential from the ammonia cracking plant to the gas compression intercoolers, water will be used just as in the CO_2 process. Energetic values for compression and cooling are shown in Table 3.

3.4. Cold storage

The last application for cold utilisation is industrial cold storage. There is one crucial difference between this application and the gas compression applications. In contrary to gas compression, cold storage (refrigerated) needs to actually be cooled to cryogenic temperatures ($-18\ ^{\circ}C$ for meat industry (Coast appliances)). In some cases, warehouses even need to be cooled to $-60\ ^{\circ}C$ (for fish) (He et al., 2019), however those cases will not be considered in this application.

4. Results

4.1. Waste heat from electrolyser

The results from the electrolysis model are presented in this section in order to check the validity and eventually for the further use in different applications. In order to check the validity of the model, different operational parameters have been compared to reference values (see Table 4). Stack efficiency can be determined with Equation (28).

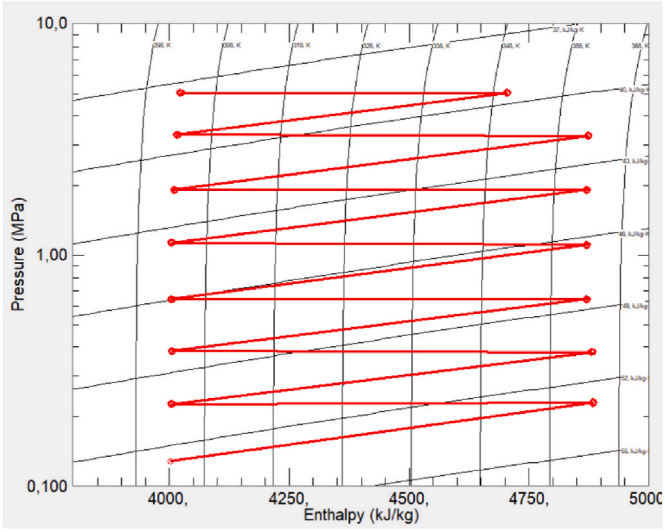

Fig. 12. Hydrogen compression process of 1–50 bar. The plot was made with NIST REFPROP (Lemmon et al., 2018).

Table 3
Energetic values for compression and cooling of H_2 for the different cases. Specific energy has been determined with Fig. 12 and H_2 massflow of 6.69 kg/s is used from the electrolysis model. For the power calculation of the cooling energy, a COP of 3.78 is used (Jackson and Brodal, 2018). Power and yearly usage show the electrical energy needed.

	Δh H_2	mean power	yearly usage
Compression	5833.1 kJ/kg	39.0 MW	3.42e+5 MWh
Cooling	5811.6 kJ/kg	10.30 MW	9.04e+4 MWh

Table 4
Comparison of efficiency values of model and literature. The model values are at 353 K and 1.3 A/m^2.

Parameter	value model	value reference
Stack eff. (LHV)	63.8 %	63–71 % (Buttler and Spliethoff, 2018)
Stack eff. (HHV)	72.2 %	80 % (ISPT et al., 2023)
Specific power use	4.66 kWh/Nm^3	4.2–4.8 kWh/Nm^3 (Buttler and Spliethoff, 2018)
H_2 production	4527 Nm^3/h	4000 (Thyssenkrupp nucera, 2023) to 4460 Nm^3/h (ISPT et al., 2023)
Cold start up time	15 min	<30 (Deng et al., 2024) to 120 min (Buttler and Spliethoff, 2018)

$$\epsilon = \frac{\dot{V}_{H2}\ HHV}{P_{electrical}} \tag{28}$$

Comparing the modelled values with the reference values, it is noticeable that efficiency is relatively low. Note that, although the model has been based on a 20 MW reference, the actual nominal capacity is 22.3 MW. This results in higher current density, thus more overpotential and lower efficiency. Furthermore, this higher nominal capacity results in more H_2 production than that of the reference case. Lastly, the start-up time is on the lower end of the spectrum. This fast start up time is expected for modern alkaline electrolysers. However, it was also noticed that changes with the start-up time resulted in negligible changes of produced waste heat in this model. The precision of this model was analyzed by comparing the steady state model output with the expected waste heat using Equation (28), which resulted in a deviation of 0.2 %.

Following this successful validation, the model is used to ascertain the actual amount of waste heat. The annual amount of fractional waste heat from the electrolyser model is represented in Fig. 13 which corresponds to the intermittent electrolyser operation due to RES. As seen, 16.6 % of the input energy is converted to useable waste heat (excluding waste heat that is reused for preheating process water). The same analysis has been done with a steady state operation for comparison. In the steady state operation 11.2 % more waste heat is produced (compared to unsteady operation). This can be attributed to the efficiency curve of the electrolyser; at lower current densities, the efficiency is higher, thus less waste heat is produced. The total amount generated waste heat, for the entire 2 GW expected nominal capacity, results in Fig. 14.

4.2. Ammonia cracking

The total efficiency of the process can be defined in several ways, here Equation (29) is used. The lower heating value (LHV) of hydrogen is 120 MJ/kg and of ammonia 18.8 kJ/kg. The efficiency of the process that is modelled is 90.3 %. The process that has been used as a reference has an efficiency of 89 %. The modelled efficiency is a bit higher than the reference, which could be expected as the air-fuel ratio is not stoichiometric in reality

The constructed composite curve (Fig. 6) can now be used to determine if and how much heating can be integrated and how much cooling

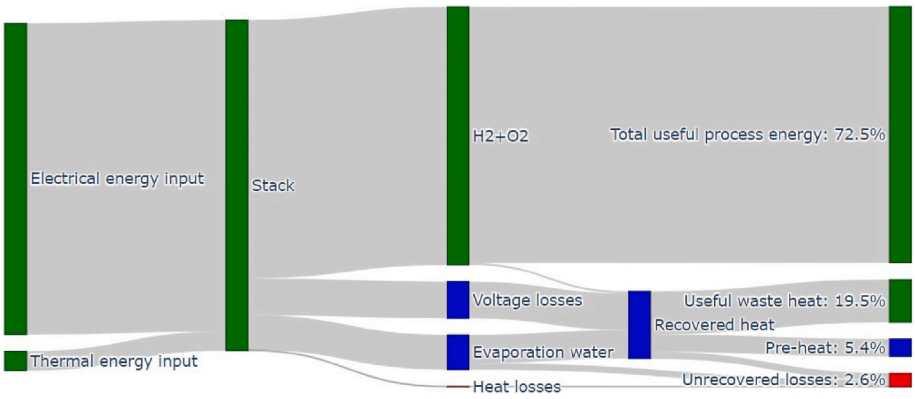

Fig. 13. Sankey diagram representing the electrolysis process.

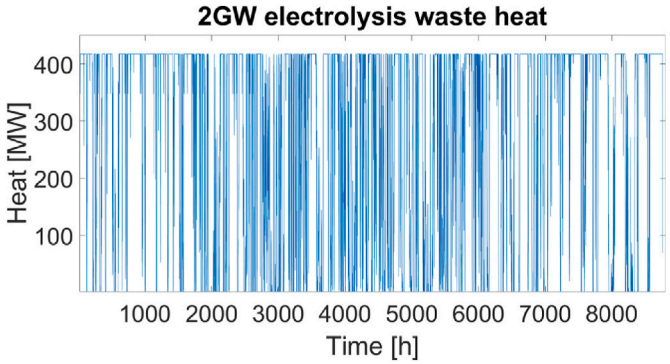

Fig. 14. Waste heat produced by 2 GW electrolysis powered by wind power.

can be provided. The maximum amount of heating/cooling will be limited by the pinch point in the composite curve; here a pinch temperature of 5 K is used. In order to integrate different thermal streams in the composite curve, the temperature range of these streams are needed. The electrolysis waste heat is integrated from 70 to 40 $^{\circ}C$ as explained in the electrolyser model. To determine the maximum amount of cooling that can be delivered to the gas compression and cold storage, an approach temperature of 5 K is assumed. This results in the temperature ranges as shown in Table 5 and Fig. 15.

If the assumption is made that a decrease in hot utility directly translates to an efficiency increase, it would correspond to 51.6 MW/% for a single ammonia cracking plant. This analysis has been done for a 2.92 kt/day hydrogen (=1.06 Mt/year), which is 23 % of what Port of Rotterdam Authority is expecting in 2030. This means 4 to 5 of these plants would be operational, providing 11.00 PJ/year of cooling and 12.38 PJ/year of potential waste heat integration (for 30 bar NH_3) by 2030.

$$\eta = \frac{\dot{m}_{H2}\ LHV_{H2}}{\dot{m}_{NH3}\ LHV_{NH3}} \tag{29}$$

Table 5
Amount of heat that can be integrated into the modelled ammonia cracking plant for the different studied temperature ranges (with corresponding efficiency increase).

Temperature range [°C]	Heat integration	Application
40 to 70	98 MW	Electrolysis
5 to 64	99 MW	CO_2
25 to 89	144 MW	H_2
−28 to −18	13 MW	Cold storage

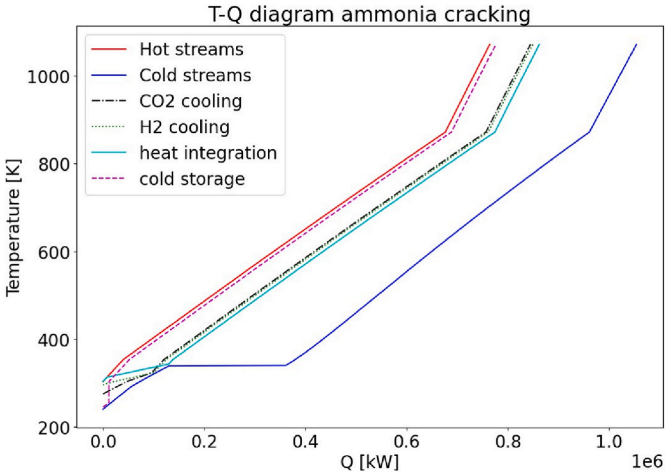

Fig. 15. Composite curve with integrated streams.

4.3. District heating

4.3.1. Urban areas

The results are shown in a load duration curve as presented in Fig. 16. As can be seen, the electrolysis waste heat can provide 72 % of the heat demand on a yearly basis for urban areas with district heating. The other 28 % needs to be supplied by an ancillary flexible heating source. From the perspective of the heat demand, this is quite a large fraction. However, this amount of energy accounts for only 10 % of the total available waste heat.

4.3.2. Greenhouses

The results are shown in a load duration curve as presented in Fig. 17. As seen, the electrolysis waste heat can provide 31 % of the heat demand on a yearly basis for urban areas with district heating. The other 69 % needs to be supplied by an ancillary flexible heating source. This amount of energy accounts for 70 % of the total available waste heat.

4.4. Ammonia cracking heat integration

It was concluded that a maximum of 98 MW of waste heat integration can be accommodated by the modelled ammonia cracker (within electrolysis waste heat temperature range). If the total amount of possible heat would be integrated in this range, this could potentially increase cracking efficiency by 2 %. With the steady state assumption and the total expected capacity of ammonia cracking within the port of Rotterdam (capacity of 4.35x the modelled plant), this translates to 426 MW of theoretical heat uptake capacity in total (13.4 PJ/year). The expected 2

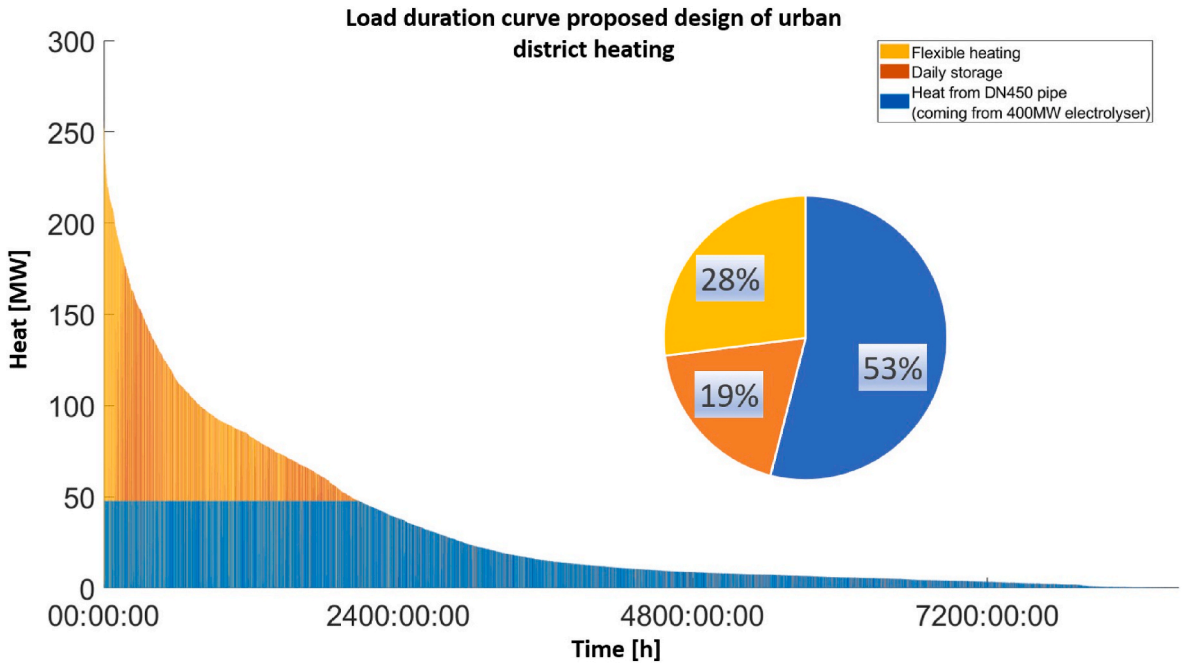

Fig. 16. Load duration curve for heat supply to urban area.

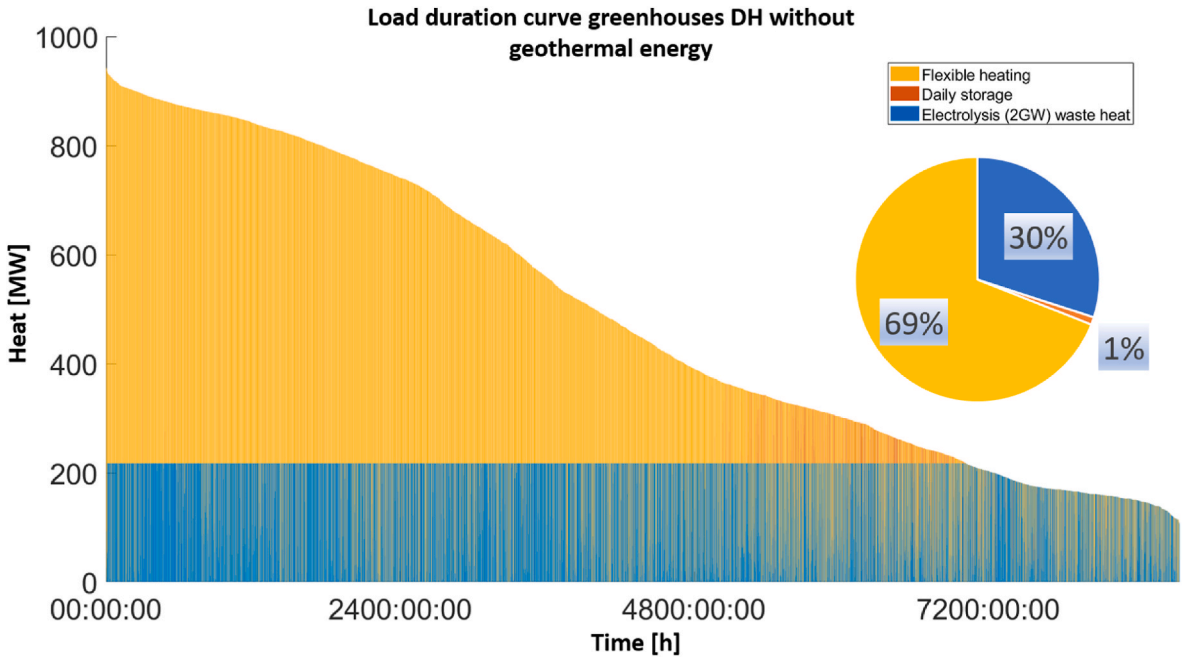

Fig. 17. Load duration curve for heat supply to greenhouses.

GW of electrolysis generates 433 MW of heat at nominal (maximum) capacity and 7.0 PJ/year in total. Although on a yearly basis, there might be enough capacity to integrate all of the waste heat, the electrolysis has higher peaks. The results are shown in Table 6.

4.5. Gas compression intercooling

4.5.1. CO_2

In this case, 115 kg/s of cooling water is used (see Table 7). From Table 5 and Fig. 15 it was determined that 400 kg/s could be accommodated per plant (thus 1740 kg/s total). This means only 6.6 % of the total available capacity is utilised, potentially increasing cracking

Table 6
Results of integrating electrolysis waste heat in ammonia cracking process. The heat reused shows how much waste heat from the 2 GW electrolysis process is reused. The efficiency increase is the potential efficiency increase of the ammonia cracking plant. Storage used is 1.09 GWh.

	Heat [GWh/year]	Heat reused	Efficiency increase
Available heat	1950		
Actual integrated:			
With storage	1906	98 %	1.0 %
Without storage	1816	93 %	0.9 %

Table 7
Final mass and energy flow values for exchanging heat in CO_2 compression process. The pressure of ammonia is 30 bar.

	CO_2 side	Water	NH_3 side
Massflow	79.3 kg/s	115.0 kg/s	65.7 kg/s
Δh	291.41 kJ/kg	200.9 kJ/kg	352 kJ/kg

efficiency by 0.1 %. It can therefore be concluded that there is more than enough capacity to accommodate this cooling application. By utilising the cooling from ammonia cracking, the electrical energy use of the CO_2 compression decreases by 61 %.

4.5.2. H_2

In this case, 197.7 kg/s of cooling water is used (see Table 8). From Table 5 and Fig. 15 it was determined that 540 kg/s of cooling water in the temperature range of 25–89 $^{\circ}C$ can be integrated in the ammonia cracking process per plant (thus 2349 kg/s total). This means that with the expected capacity, only 8.4 % of the total available cooling capacity would be used. Potentially increasing cracking efficiency by 0.2 %. It can therefore be concluded that there is more than enough capacity to accommodate this cooling application. By utilising the cooling from ammonia cracking, the electrical energy use of the H_2 compression decreases by 21 %.

4.6. Cold storage

From Tables 5, it was determined that 13 MW of cooling can be delivered for cold storage with one ammonia cracking plant. For the total amount of expected cracking plants, this would be 56.6 MW. The relation of Equation (30) (Nunes et al., 2014) is used to determine how much cold storage can be cooled with this, E is the electricity consumption per year (MWh) and V the storage volume (m^3). Assuming a COP of 3.78 for the cooling (Jackson and Brodal, 2018), the volume can be re-written to Equation (31).

$$E = 0.3143\ V - 6.84 \tag{30}$$

$$V = 0.842\ E + 21.76 \tag{31}$$

This results in a cold storage volume of 417546 m^3. Which would be enough to cool a few cold rooms considering a typical storage volume of 10–11 000 m^3 (Nunes et al., 2014).

5. Discussion

5.1. Electrolysis waste heat utilisation

Integration of electrolysis waste heat in district heating was compared with integrating it in ammonia cracking. Comparing the result from both applications, it is observed that much more heat can be integrated in ammonia cracking compared to district heating (98 % in ammonia cracking directly, 11 % and 72 % for different district heating cases). Only based on those numbers it would appear that ammonia cracking heat integration has the advantage. It could be argued that only a specific case is considered and that this may not generally be the case.

It is true that if more (green)houses would be considered for district heating, that the percentage of reused heat would increase. This would, however, call for extensive infrastructure which can outweigh the benefit. One of the advantages of integrating heat to ammonia cracking is that it is expected to be a steady process, in contrary to the fluctuating demand of a district heating network. Even without the use of buffering, the ammonia cracking heat integration potential is much larger. Moreover, the temperature restrictions on the waste heat integration are less for ammonia cracking compared to district heating. While district heating has a temperature requirement of at least 60 $^{\circ}C$, ammonia cracking heat integration does not have this restriction. This study did assume that no heat upgrading is needed for district heating, based on a simple representation of the heat transport. However, this might not be the case in reality. The losses are assumed in steady state, while the system is operating unsteady. While in times of demand the steady state assumption works well, there might be moments where heat upgrading may still be required. Thereby increasing system cost even more for district heating. No in depth economic analysis has been done for the infrastructure costs. Considering that district heating has a more complicated infrastructure in the port of Rotterdam due to long distances and existing infrastructure, compared to what is expected for ammonia cracking, it is expected that costs are higher as well (not only more, but also different types of components).Lastly by integrating waste heat from electrolysis in ammonia cracking, a synergy is created within the hydrogen value chain. Thereby potentially increasing total energy efficiency and lowering production cost, which could accelerate the transition.

A major disadvantage from using the waste heat in ammonia cracking, is that it is not directly used for decarbonisation. Modern ammonia plants are proposed to work with recycled hydrogen and ammonia from the feed stream for as a heating source. Adding waste heat would make the process more efficient, but not diminish any fossil fuels. In contrary, heating of (green)houses in the Netherlands is still mostly accomplished by burning natural gas. Here, using waste heat for district heating could directly have in impact in fossil fuel consumption. Another possible disadvantage could be potential difficulties in using the intermittent source in the steady state process of ammonia cracking. The limited increase in efficiency might not be worth it if plant control would increase drastically.

Table 8
Final mass and energy flow values for exchanging heat in H_2 compression process. The pressure of ammonia is 30 bar in this case.

	H_2 side	Water	NH_3 side
Massflow	6.69 kg/s	197.7 kg/s	85.6 kg/s
Δh	5811.6 kJ/kg	196.6 kJ/kg	454.0 kJ/kg

5.2. Ammonia cracking cold utilisation

Ammonia cracking cold utilisation is a novel topic, as are both applications that have been compared. By comparing the potential of the gas compression with cold storage, Table 5 indicates that much more thermal energy can be used in gas compression. The main reason for this, is that the cold storage application has a much more restricted temperature range, which translates in a smaller ΔT. In the specific case in the port of Rotterdam, the difference is less pronounced because the actual amount of gas that needs to be compressed (both CO_2 and H_2) is much less than what could potentially be accommodated.

The results from this study indicate that from a quantitative and qualitative perspective, thermal energy from ammonia cracking can be used for cold utilisation. However, the practical implementation has not been studied.

6. Conclusion

In this study, the potential of reusing thermal waste streams in hydrogen production and import was analyzed by comparing different known and novel applications. It has been shown that multiple applications are technically possible for reusing thermal waste streams from both low temperature water electrolysis and ammonia cracking.

The main conclusion based on the results of this study, is that there is a lot of potential for reusing low temperature electrolysis waste heat in the ammonia cracking process. 98 % of the available waste heat from 2 GW electrolysis capacity (operated by wind power) can directly be integrated in the ammonia cracking process (total capacity of 90 kt/day NH_3 input). This is much more compared to the district heating

application studied in the port area, for which 10 % could be integrated for an urban area and 70 % for greenhouses. On top of that, the district heating infrastructure is more complex than what is needed for integration in ammonia cracking. Also integrating the waste heat into ammonia cracking has less restrictions in terms of temperature than for district heating. Lastly the reuse of electrolysis waste heat in ammonia cracking forms a synergy within the hydrogen industry.

This study has also started to explore the novel field of ammonia cracking cold utilisation. Although results have shown that gas compression intercooling and industrial cold storage are applications that might technically be possible, the practical implementation needs further research. Also the total volumes of cooling needed by gas compression and cold storage applications are small compared to what could be delivered by the total ammonia cracking plants. Thus a potential efficiency advantage would also stay limited for these specific cases. This also makes it a less attractive option compared to electrolysis heat integration.

CRediT authorship contribution statement

Maxime Philip Kramer: Writing – review & editing, Writing – original draft, Visualization, Software, Resources, Methodology, Investigation, Formal analysis, Data curation, Conceptualization. **Klaas-Jan Bosch:** Writing – review & editing, Conceptualization. **Kamel Hooman:** Writing – review & editing, Conceptualization.

Declaration of competing interest

The authors declare that they have no known competing financial interests or personal relationships that could have appeared to influence the work reported in this paper.

Appendix A. Supplementary data

Supplementary data to this article can be found online at https://doi.org/10.1016/j.clet.2025.100940.

Data availability

Data was used from online open sources (links are provided in article)

References

Asif, M., Sidra Bibi, S., Ahmed, S., Irshad, M., Shakir Hussain, M., Zeb, H., Kashif Khan, M., Kim, J., 2023. Recent advances in green hydrogen production, storage and commercial-scale use via catalytic ammonia cracking. Chem. Eng. J. 473, 145381.

Aspen Technology Inc. Aspen plus v12. https://www.aspentech.com/en/products/engineering/aspen-plus, 2024.

Becker, H., Murawski, J., Shinde, D.V., Stephens, I.E.L., Hinds, G., Smith, G., 2023. Impact of impurities on water electrolysis: a review. Sustain. Energy Fuels 7, 1565–1603.

Bell, I.H., Wronski, J., Quoilin, S., Lemort, V., 2014. Pure and pseudo-pure fluid thermophysical property evaluation and the open-source thermophysical property library coolprop. Ind. Eng. Chem. Res. 53 (6), 2498–2508.

Böhm, H., Moser, S., Puschnigg, S., Zauner, A., 2021. Power-to-hydrogen and district heating: Technology-based and infrastructure oriented analysis of (future) sector coupling potentials. Int. J. Hydrogen Energy 46 (63), 31938–31951.

Buttler, A., Spliethoff, H., 2018. Current status of water electrolysis for energy storage, grid balancing and sector coupling via power-to-gas and power-to-liquids: a review. Renew. Sustain. Energy Rev. 82, 2440–2454.

Isoplus. isoplus design manual 2011 complete alle chapters-web, n.d. https://www.logstor.com/catalogues-and-documentation?lang=1737type=1613.

AGFA. Technical Data Sheet Zirfon Utp 220 Separator Membrane for Alkaline Electrolysis.

Coast appliances. freezer temperatures. https://www.coastappliances.ca/blogs/learn/freezer-temperature-guide::text=According2024.

CBS. oppervlakte westland. https://opendata.cbs.nl//CBS/nl/dataset/80781ned/table?dl=5B50E/, 2024.

De Nora, 2024. Polarisation curve denora. https://www.denora.com/applications/H2-production-by-water-electrolysis.html/.

Deng, X., Yang, F., Li, Y., Dang, J., Ouyang, M., 2024. Thermal analysis and optimization of cold-start process of alkaline water electrolysis system. In: Sun, H., Pei, W., Dong, Y., Yu, H., You, S. (Eds.), Proceedings of the 10th Hydrogen Technology Convention, vol. 1. Springer Nature Singapore, Singapore, pp. 297–311.

Desmond, C., Murphy, J., Blonk, L., and Haans, W. Description of an 8 Mw Reference Wind Turbine. 092013.

Devkota, S., Shin, B.-J., Mun, J.-H., Kang, T.-H., Yoon, H.C., Mazari, S.A., Moon, J.-H., 2023. Process design and optimization of onsite hydrogen production from ammonia: reactor design, energy saving and nox control. Fuel 342, 127879.

Diéguez, P., Ursúa, A., Sanchis, P., Sopena, C., Guelbenzu, E., Gandía, L., 2008. Thermal performance of a commercial alkaline water electrolyzer: experimental study and mathematical modeling. Int. J. Hydrogen Energy 33 (24), 7338–7354.

EHB, 2020. European hydrogen backbone report. https://ehb.eu/files/downloads/2020_European-Hydrogen-Backbone_Report.pdf, 2020.

Elsaid, K., Taha Sayed, E., Yousef, B.A., Kamal Hussien Rabaia, M., Ali Abdelkareem, M., Olabi, A., 2020. Recent progress on the utilization of waste heat for desalination: a review. Energy Convers. Manag. 221, 113105.

Fluor. Port of rotterdam prefeasibility study large scale ammonia cracking, Internal Document Port of Rotterdam, 2023.

Gasunie, 2024. Hydrogen import. https://www.gasunie.nl/en/expertise/hydrogen/hydrogen-import.

González, D., Amigo, J., Suárez, F., 2017. Membrane distillation: Perspectives for sustainable and improved desalination. Renew. Sustain. Energy Rev. 80, 238–259.

Haverkort, W. Electrolysers, 2024. Fuel Cells and Batteries: Analytical Modelling. TU Delft open.

He, T., Chong, Z.R., Zheng, J., Ju, Y., Linga, P., 2019. Lng cold energy utilization: prospects and challenges. Energy 170, 557–568.

Hermans, Ewoud, 2022. Extracting and Utilising Heat from an Hydrogen Production Plant. Student Paper.

Hu, S., Guo, B., Ding, S., Yang, F., Dang, J., Liu, B., Gu, J., Ma, J., Ouyang, M., 2022. A comprehensive review of alkaline water electrolysis mathematical modeling. Appl. Energy 327, 120099.

Hynetwork, 2024. Hynetwork pressure specifications. https://www.hynetwork.nl/en/business/become-a-customer/specifications.

Irena, 2023. World energy transitions outlook 2023. https://www.irena.org/Publications/2023/Jun/World-Energy-Transitions-Outlook-2023.

ISPT, van het Noordende, H., Ripson, P., 2023. 1 gigawatt green hydrogen plant. https://ispt.eu/publications/a-one-gigawatt-green-hydrogen-plant/.

Jackson, S., Brodal, E., 2018. A comparison of the energy consumption for co2 compression process alternatives. IOP Conf. Ser. Earth Environ. Sci. 167 (1), 012031.

Kanbur, B.B., Xiang, L., Dubey, S., Choo, F.H., Duan, F., 2017. Cold utilization systems of lng: a review. Renew. Sustain. Energy Rev. 79, 1171–1188.

Kayali, Fawzi, 2023. Integrating Waste Heat from Hydrogen Production into District Heating. Student Paper.

Le Coultre, F.S., 2022. Utilisation of Heat Released during the Production of Green Hydrogen Using Alkaline Electrolysis. Student Paper.

Lemmon, E.W., Bell, I.H., Huber, M.L., McLinden, M.O., 2018. NIST Standard Reference Database 23: Reference Fluid Thermodynamic and Transport Properties-REFPROP. National Institute of Standards and Technology, Version 10.0.

Lu, J., Li, Y., Li, B., Yang, Q., Deng, F., 2023. Research on re-liquefaction of cargo bog using liquid ammonia cold energy on co2 transport ship. Int. J. Greenh. Gas Control 129, 103994.

Maxwell, G.R., 2004. Uses of ammonia. Synthetic Nitrogen Products: A Practical Guide to the Products and Processes, pp. 199–203.

Nunes, J., Neves, D., Gaspar, P.D., Silva, P.D., Andrade, L.P., 2014. Predictive tool of energy performance of cold storage in agrifood industries: the Portuguese case study. Energy Convers. Manag. 88, 758–767.

Olivier, P., Bourasseau, C., Bouamama, P.B., 2017. Low-temperature electrolysis system modelling: a review. Renew. Sustain. Energy Rev. 78, 280–300.

Østergaard, P.A., Andersen, A.N., 2023. Optimal heat storage in district energy plants with heat pumps and electrolysers. Energy 275, 127423.

Port of Rotterdam, 2024. Ammonia import need. https://www.portofrotterdam.com/en/port-future/energy-transition/ongoing-projects/hydrogen-rotterdam/import-of-hydrogen.

Port of Rotterdam, 2025a. Hydrogen plans. https://www.portofrotterdam.com/sites/default/files/2024-05/developing-europes-hydrogen-hub.pdf.

Port of Rotterdam, 2025b. Hydrogen plans. https://www.portofrotterdam.com/sites/default/files/2021-06/hydrogen-economy-in-rotterdam-handout.pdf.

Porthos. Porthos info. https://www.porthosco2.nl/project/, 2024.

Pozzetto, Alessandro, 2022. Distribution Grid Planning Considering Sector Coupling and Waste Heat Recovery. Student Paper.

Reuter, S., Schmidt, R.-R., 2022. Assessment of the future waste heat potential from electrolysers and its utilisation in district heating. In: NEFI Conference Proceedings, pp. 41–51. NEFI-Conference ; Conference date: 13-10-2022 Through 14-10-2022.

Royal haskoning, D.H.V., 2022. Haalbaarheidsstudie gebruik industriële restwarmte europoort/maasvlakte. Internal Document Port of Rotterdam.

Sakas, G., Ibáñez-Rioja, A., Ruuskanen, V., Kosonen, A., Ahola, J., Bergmann, O., 2022. Dynamic energy and mass balance model for an industrial alkaline water electrolyzer plant process. Int. J. Hydrogen Energy 47 (7), 4328–4345.

Sakas, G., Ibáñez-Rioja, A., Pöyhönen, S., Järvinen, L., Kosonen, A., Ruuskanen, V., Kauranen, P., Ahola, J., 2024. Sensitivity analysis of the process conditions affecting the shunt currents and the sec in an industrial-scale alkaline water electrolyzer plant. Appl. Energy 359, 122732.

Sanchuli, N., Dan, S., Bagheri, H., 2024. Chapter six - ammonia application in cooling systems. In: Basile, A., Rahimpour, M.R. (Eds.), Progresses in Ammonia: Science, Technology and Membranes. Elsevier, pp. 113–132.

Sdanghi, G., Maranzana, G., Celzard, A., Fierro, V., 2019. Review of the current technologies and performances of hydrogen compression for stationary and automotive applications. Renew. Sustain. Energy Rev. 102, 150–170.
Sommer Hansen, Søren, Dokkedal Johnsen, Emil, 2023. Integration of Waste Heat from Power to X in District Heating Systems. Student Paper.
Thoughtco. steel conductivity. https://www.thoughtco.com/table-of-electrical-resistivity-conductivity-608499/, 2024.
Thyssenkrupp nucera, 2023. Industrial-scale water electrolysis for green hydrogen production. https://thyssenkrupp-nucera.com/wp-content/uploads/2023/11/thyssenkrupp-nucera_green-hydrogen_brochure_web.pdf.
Tiktak, Joris, 2019. Heat Management of PEM Electrolysis A study on the potential of excess heat from medium- to large-scale PEM electrolysis and the performance analysis of a dedicated cooling system. Student Paper. https://repository.tudelft.nl/record/uuid:c046820a-72bc-4f05-b72d-e60a3ecb8c89.
TNO. Offshore wind data. https://offshorewind-measurements.tno.nl/en/data/, 2024.
TNO. Warmteprofielengenerator. https://www.warmteprofielengenerator.nl, 2022.
van der Roest, E., Bol, R., Fens, T., van Wijk, A., 2023. Utilisation of waste heat from pem electrolysers – unlocking local optimisation. Int. J. Hydrogen Energy 48 (72), 27872–27891.
Vidisdottir, Dis, Elena, 2022. Profitability of Green Hydrogen Production and Feasibility of Waste Heat Integration to DHS in the Ísafjörð Ur's Energy System: A Techno-Economic Analysis. Student Paper.
Witkowski, A., Rusin, A., Majkut, M., Stolecka, K., 2017. Comprehensive analysis of hydrogen compression and pipeline transportation from thermodynamics and safety aspects. Energy 141, 2508–2518.
Yodwong, B., Guilbert, D., Phattanasak, M., Kaewmanee, W., Hinaje, M., Vitale, G., 2020. Faraday's efficiency modeling of a proton exchange membrane electrolyzer based on experimental data. Energies 13, 18.
ZareNezhad, B., Aminian, A., 2011. Accurate prediction of the dew points of acidic combustion gases by using an artificial neural network model. Energy Convers. Manag. 52 (2), 911–916.
Zhang, G., Liu, Z., Zhang, X., Yang, Y., 2023. Study on fuel cold energy utilization of large ammonia powered ship. IOP Conf. Ser. Earth Environ. Sci. 1171 (1), 012026.